

Cloud modulation of surface solar irradiance at a pasture site in southern Brazil

Lianhong Gu^{a,*}, Jose D. Fuentes^a, Michael Garstang^a, Julio Tota da Silva^b,
Ryan Heitz^a, Jeff Sigler^a, Herman H. Shugart^a

^a Department of Environmental Sciences, University of Virginia, Charlottesville, Virginia 22903, USA

^b Centro de Previsão de Tempo e Estudos Climáticos (CPTEC), Instituto Nacional de Pesquisas Espaciais (INPE), Rodovia Presidente Dutra Km 40, Cachoeira Paulista, São Paulo, Brazil

Received 7 February 2000; received in revised form 1 August 2000; accepted 10 August 2000

Abstract

Broken cloud fields create mosaic radiative landscapes with interchanging cloud-shaded and sunlit areas. While clouds attenuate solar radiation incident on cloud-shaded areas, sunlit ground surfaces may actually receive more irradiance than under a clear sky due to light scattering and reflection from neighboring clouds. In this paper, we studied these two opposite but closely related aspects of cloud modulation of surface solar irradiance at a pasture site in southern Brazil. We analyzed a high-resolution time series of surface measurements obtained during the 1999 wet season. Surface solar irradiance frequently (more than 20% of the time) exceeded clear-sky levels and occasionally surpassed the extraterrestrial radiation. Clouds created a bimodal frequency distribution of surface solar irradiance, producing an average of approximately 50 and 14% for attenuation and enhancement, respectively, as compared to corresponding clear-sky level irradiance. The average duration of enhancement periods was about 1/3 of the average duration of attenuation periods. On the daily basis, cloud-induced enhancement contributed an average of 4% of the daily solar input to the surface and compensated for more than 10% of the attenuation due to the presence of clouds. Through spectral analysis, two temporal regimes were shown to modulate the surface irradiance by clouds. One was a convective/mesoscale of tens of minutes to hours and the other was a turbulent scale of several minutes corresponding to the classical Kolmogorov $f^{-5/3}$ power law. © 2001 Elsevier Science B.V. All rights reserved.

Keywords: Solar irradiance; Cloud gap effect; Tropical clouds; Convective regime; Turbulence diffusion regime; Kolmogorov power law

1. Introduction

Large spatial heterogeneity in solar radiative forcing can be created when clouds do not continuously cover the underlying surface. Interchanging cloud-shaded

and sunlit areas form a mosaic landscape of surface solar irradiance. What makes this picture interesting is that sunlit ground surfaces may actually receive more irradiance than under a clear sky. This is possible because sunlit ground surfaces, which are located at the end of the paths of solar beams passing through gaps formed by individual clouds in neighboring skies, receive the same amount of direct radiation as under the clear sky, while the diffuse radiation component is increased due to light scattering and reflection from neighboring clouds (Segal and Davis, 1992; Duchon

* Corresponding author. Present address: Department of Environmental Science, Policy and Management, Ecosystems Science Division, University of California, Berkeley, 151 Hilgard Hall, Berkeley, CA 94720-3110, USA.

E-mail address: lianhong@nature.berkeley.edu (L. Gu).

and O'Malley, 1999; Gu et al., 1999). This phenomenon has been termed 'cumulus solar-irradiance reflection' (Segal and Davis, 1992) and the 'cloud gap effect' (Gu et al., 1999). In this paper, we adopt the term 'cloud gap effect' to denote the cloud-induced enhancement of surface irradiance. We argue that cumulus clouds are not the only cloud type that can enhance surface solar irradiance. With proper solar elevation angles, any gaps in cloud cover can create areas on the ground surface where solar irradiance exceeds the clear-sky level because of the increased contribution from the diffuse radiation. However, we concur with earlier studies (Segal and Davis, 1992) that clouds with large vertical development such as cumulus and cumulonimbus are the most favorable ones due to their discontinuity in covering the underlying surface and well-shaped walls for effective light reflection.

Direct analyses of a mosaic radiative landscape are difficult because the radiation field at this scale cannot be readily obtained. Alternatively the phenomenon can be studied in the time domain. For a fixed point on the ground, the surface may experience alternatively sunlit and shaded conditions due to the movement of the cloud field and changes in solar elevation angles. This leads to a time series of the received solar irradiance that is characterized by alternative periods of reduced solar radiation and unusually high solar radiation. Such a feature is commonly observed in high time resolution pyranometer records (Segal and Davis, 1992).

Segal and Davis (1992) evaluated the magnitude of the cloud gap effect using measurements obtained along the Front Range of Colorado, USA. They reported that the cloud gap effect was able to cause increases of up to $\sim 250 \text{ Wm}^{-2}$ in surface solar irradiance with periods lasting 15–30 min. Gu et al. (1999) analyzed data given in Duchon and O'Malley (1999) for Lamont, Oklahoma, USA and found that around noontime the cloud gap effect can increase ground surface irradiance by more than 20% over the clear-sky level. To our knowledge, no studies have been conducted to evaluate the magnitude and dynamic characteristics of the cloud gap effect in the tropics of prevailing cumuliform clouds where some of the most magnificent clouds in the world are often observed (Garstang and Fitzjarrald, 1999).

In this study, we report the results of a detailed study of a high-resolution time series of surface solar irradiance obtained from a pasture area in Brazil during the 1999 wet season. The main objectives of this study are: (1) to investigate the statistical characteristics (magnitude, duration and frequency) of the cloud gap effect as well as cloud irradiance attenuation and associated cloud types, (2) to ascertain the influence of the dual functions of clouds (radiation attenuation and enhancement) on solar radiative forcing on a daily basis, and (3) to determine scaling properties of the temporal dynamics of surface solar irradiance modulated by clouds. The findings reported here have direct application to processes requiring solar energy. Examples include stomatal dynamics and associated plant carbon dioxide uptake and transpiration, emissions of phytogenic hydrocarbons, and photolysis of a plethora of airborne molecules.

2. Site description and measurements

Measurements were made at a pasture site in the state of Rondônia, Brazil ($10^{\circ}45'S$, $62^{\circ}22'W$) during January and February 1999. This period corresponded to the rainy season. The site is part of a large deforested area dominated by short grass with palm and isolated trees scattered throughout the landscape. A fully instrumented 10 m micrometeorological tower with radiometers was set up and the continuous measurements used to characterize the local energy balance. Incoming total solar radiation was measured with two duplicating pyranometers (model PSP Eppley pyranometer, Newport, RI; model CM3, Kipp and Zonen, Holland). Outgoing total short-wave radiation was also measured with the CM3 instrument. Incoming and outgoing long-wave radiation were measured with pyrgeometers (Kipp and Zonen). Incoming and outgoing photosynthetically active radiation (PAR, Model LI190SA, LiCor Inc., Lincoln, NB) were also measured. Data were acquired using data loggers (model CR7, Campbell Scientific Inc., Logan, UT) that provided 1 min averaged quantities. In the data analyses reported below, we utilize the high-frequency, 1 min data. During the 2-month period of the field campaign, we also observed cloud types every 3 h.

3. Clear-sky irradiance model

A major step in our analyses was to determine the clear-sky solar irradiance on the ground surface so that a reference could be established for cloudy sky conditions. During the 2-month measurement period, we never observed a single completely clear day. Therefore, we applied the clear-sky solar irradiance model developed by Meyers and Dale (1983). We determined the model parameters by fitting measurements from those daily segments in which we observed no clouds directly over the site. For completeness, we outline the model here. Complete model details can be found elsewhere (e.g. Meyers and Dale, 1983; Iqbal, 1983; Duchon and O'Malley, 1999).

In the absence of clouds, the clear-sky surface irradiance I_c is determined by the product of four transmission coefficients characterizing Rayleigh scattering (t_R), permanent gas absorption (t_g), water vapor absorption (t_w), and aerosol scattering (t_a), respectively

$$I_c = I_0 t_R t_g t_w t_a \quad (1)$$

where I_0 is the extraterrestrial solar irradiance at a plane parallel to the Earth's surface. I_0 is given by

$$I_0 = I_{sc} \left[1 + 0.033 \cos \left(\frac{360D}{365} \right) \right] \sin \beta \quad (2)$$

where I_{sc} denotes the solar constant, D the day of the year, and β is the solar elevation angle. We implemented an algorithm described in Michalsky (1988) to calculate β . The product of t_R and t_g is predicted from the surface pressure p (kPa) and the optical air mass number m at 101.3 kPa by (3)

$$t_R t_g = 1.021 - 0.084 \left[m \left(949p \times 10^{-5} + 0.051 \right) \right]^{1/2} \quad (3)$$

where

$$m = 35 \left(1224 \sin^2 \beta + 1 \right)^{-1/2} \quad (4)$$

The water vapor transmission coefficient t_w is related to the atmospheric column precipitable water u (cm) and m by (5):

$$t_w = 1 - 0.077(um)^{0.3}, \quad (5a)$$

$$u = \exp(0.1133 - \ln(\lambda + 1) + 0.0393T_d) \quad (5b)$$

where T_d is the dew point temperature ($^{\circ}\text{F}$) and λ is an empirical constant based on season and latitude. The aerosol transmission coefficient t_a is given by

$$t_a = x^m \quad (6)$$

where x is an empirically determined coefficient.

For the Northern Hemisphere, values for λ and x can be found in the literature (e.g. Smith, 1966; Meyers and Dale, 1983; Duchon and O'Malley, 1999). For the Southern Hemisphere, however, we do not know their values. To determine λ and x for our site, we constructed a minimization function to be applied for those daily periods in which we observed no clouds

$$f(\lambda, x) = \frac{1}{n} \sum_{i=1}^n (I_i - I_{ci})^2 \quad (7)$$

where I_i s are solar irradiance measurements from those periods for which no clouds were observed directly over the site, n is the total number of measurements, and I_{ci} s are corresponding model results when λ and x are given. We minimized the function $f(\lambda, x)$ by using the conjugate gradient method (Press et al., 1992). The values we obtained are $\lambda = 2.80$, and $x = 0.925$. As shown in Fig. 1, fitted model results agree closely with measured clear-sky surface irradiance.

Obviously for the treatment employed here one can always ask the following question: how is the enhancement during the 'between-clouds' periods

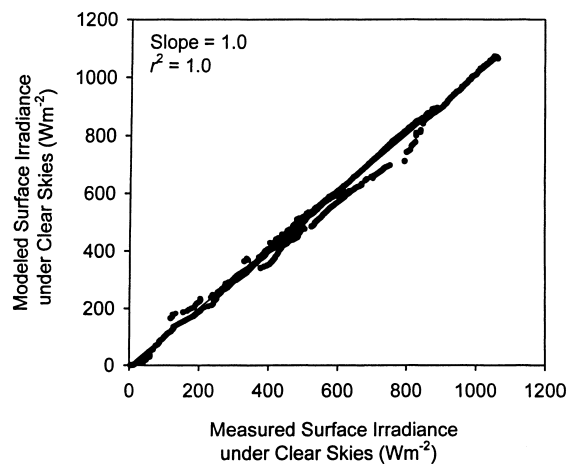


Fig. 1. Predicted and measured clear-sky surface solar irradiance.

avoided? With cloud fields located in the horizon (but not over the measurement site), there is always a possibility of surface irradiance enhancement at the place, where the sensors are located. To minimize this uncertainty, we set the following standards for the periods used in the clear-sky irradiance model: (a) the periods must be longer than 2 h; (b) the surface irradiance must follow the trend of extraterrestrial radiation and change smoothly with time. This procedure does not completely eliminate the possibility of contaminated ‘between-clouds’ periods and it is possible that the modeled clear-sky irradiance may be slightly higher than the actual value. But it ensures that the enhancement effects of clouds will not be overestimated. To further assess this issue, we compared predicted clear-sky irradiance with measured values for those clear-sky periods that were longer than 1 h but shorter than 2 h and, therefore, not used in the parameter estimation. We found good agreement between predicted and measured results ($r^2 = 0.99$, root mean square error = 29.1 Wm^{-2}). This additional test indicates that the clear-sky irradiance contamination is unlikely a problem for our analyses. It also served as an independent validation for the model and its parameter estimation because it used a different set of measurements. It is reassuring that our estimated values for λ and x are comparable to those reported in the literature for low latitudes in the northern hemisphere (Smith, 1966; Meyers and Dale, 1983).

4. Results

4.1. General features of temporal variations of surface irradiance

A striking feature in our measurements is that surface irradiance frequently surpassed the corresponding clear-sky irradiance level, and instantaneously exceeded the extraterrestrial solar radiation on many occasions. This phenomenon is confirmed by both duplicating pyranometers, which gave almost identical measurements. The cloud-induced irradiance enhancement was observed almost every day during the 2-month measurement period except for a few completely overcast days. Fig. 2 gives two examples of daily temporal changes of surface irradiance under cloudy conditions (day 35 and 38). Observed weather

elements are marked on the time (x -) axis. Also shown in the figure are clear-sky and extraterrestrial solar irradiance. In general, large enhancement occurred with cloud cover around 4/8 to 6/8, which corresponds to partly (scattered) to mostly (broken) cloudy conditions. Under these circumstances, cumulus clouds were often found dominating the sky but other types of clouds such as altocumulus, stratocumulus and altostratus were often present in the sky as well. Other features worth noting include the following.

1. Enhancement of surface irradiance was generally associated with erratic fluctuations in the time series. Extremely high irradiance values were often preceded and followed by large drops in surface irradiance, indicating the presence and movement of thick and broken clouds. Smoothly changing or slightly fluctuating measurements rarely showed irradiance enhancement. In the latter case, the modeled clear-sky irradiance curves served as the outer boundary of the small fluctuations.
2. The magnitude of the fluctuation, that is, the difference between local minima and maxima of successive shaded and sunlit periods, can exceed the magnitude of the corresponding clear-sky surface irradiance.
3. The irradiance enhancement occurred not only around noontime but also in early morning or late afternoon. This is in contrast to what was reported by Segal and Davis (1992) for the Front Range of Colorado, USA where enhancement was observed only around noontime.
4. The erratic fluctuations and enhancement of surface irradiance can occur before and after a long period of reduced surface solar radiation, indicating the presence of advancing and departing large optically thick clouds near times when enhanced irradiance was observed (e.g. during 13–14 h of day-35, Fig. 2).

4.2. Bimodality in relative changes of surface solar irradiance

We also studied the distribution of the relative changes of surface solar irradiance under the impacts of clouds. The relative change r is calculated by

$$r = 100 \times \left(\frac{I - I_c}{I_c} \right) \quad (8)$$

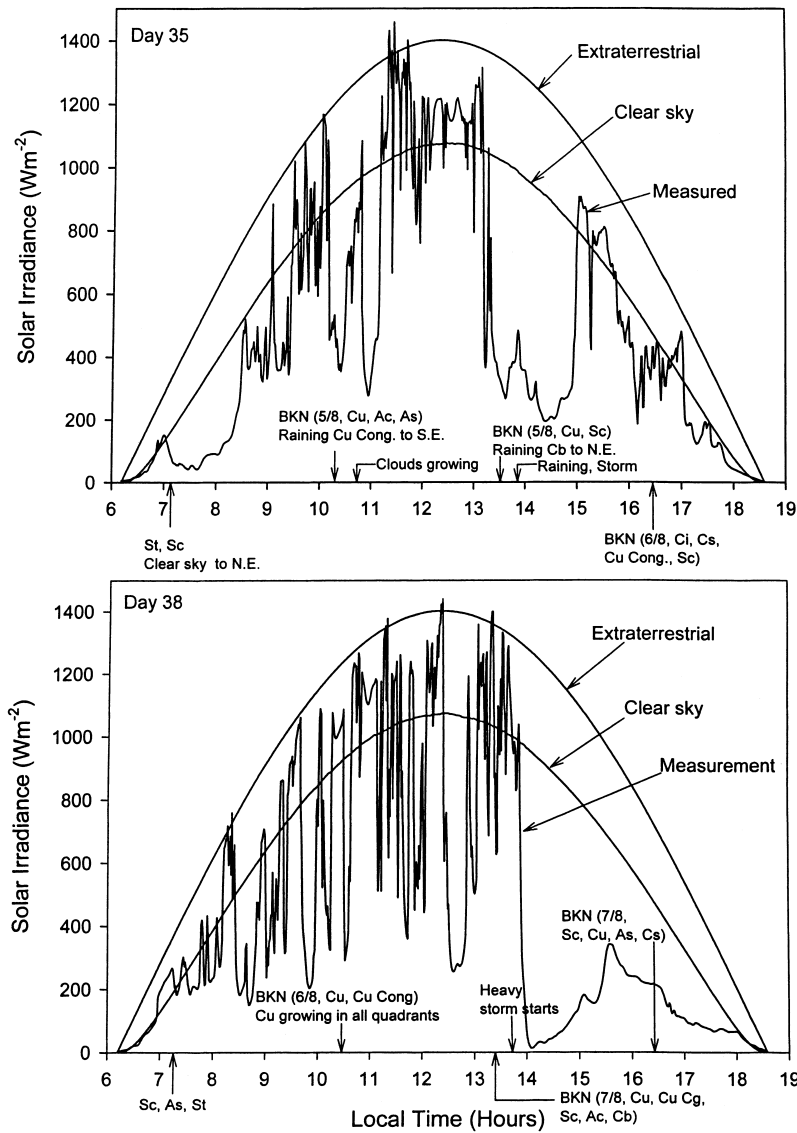


Fig. 2. Examples of the temporal changes of surface solar irradiance under partly cloudy conditions. Also shown are calculated clear-sky surface solar irradiance and extraterrestrial solar irradiance. Observed sky conditions are marked on the x-axis. The abbreviations included in the figure are defined as follows: BKN broken (clouds); Cu cumulus clouds; Ac altostratus; As altostratus; Sc stratocumulus; St stratus; Cb cumulus congestus; Ci cirrus; Cs cirrus stratus.

where I is the measured surface solar irradiance. To avoid the potential problems in sensor responses to low β , in the analyses we excluded data with $\beta < 5^\circ$. We, then, calculated the probability density function $p(r)$ for the distribution of r from the measurements obtained during the 2-month field campaign. The prob-

ability density $p(r)$ is defined by

$$p(r) = \frac{n_{r \rightarrow r+\Delta r}}{N \Delta r} \tag{9}$$

where N is the total number of measurements and $n_{r \rightarrow r+\Delta r}$ is the number of measurements with the

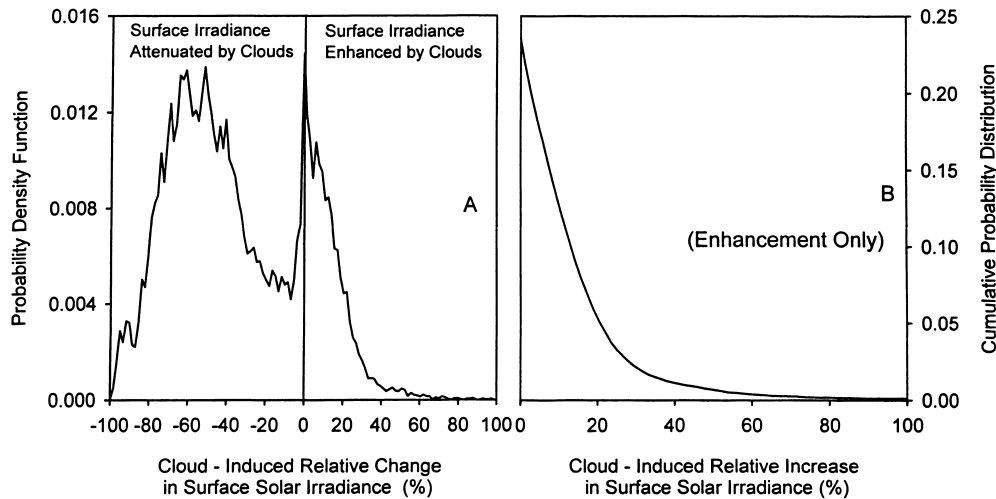


Fig. 3. Probability density function (A) and cumulative probability distribution (B) of cloud-induced changes in surface solar irradiance relative to the clear-sky level. Analyses used all measurements without regard to the time of day.

relative changes falling into the interval $(r, r + \Delta r)$. From Eq. (9), we defined the cumulative probability distribution $F(r)$ as in Eq. (10):

$$F(r) = \int_r^{+\infty} p(z) dz \quad (10)$$

$F(r)$ represents the probability that the relative change in surface irradiance exceeds a given value r . For the $F(r)$, we are only interested in $r > 0\%$ (enhancement). Fig. 3 shows the results for the probability density function (Fig. 3(A)) and the cumulative probability distribution (Fig. 3(B)) derived from the measurements. A key feature of the probability density function (Fig. 3(A)) is that it has a bimodal pattern. A broad peak is located at the negative side (reduced irradiance, negative scale on the x -axis) and centered at $r \sim -60\%$, indicating that dominant clouds overhead the measurement point substantially attenuated light levels reaching the surface. A sharp peak is located around the clear-sky irradiance level (0%) but with a long tail in the enhancement side (positive scale on the x -axis). There is a steep drop in the magnitude of the probability density function as r changes from positive to negative. For convenience in expression, we shall call the peak at the negative side the shade peak and the peak around the clear-sky irradiance level the shine peak.

The cumulative probability distribution shows that the frequency of irradiance enhancement by clouds is

fairly high (Fig. 3(B)). More than 20% of our irradiance measurements are enhanced measurements. The average r for the enhancement is 14.3%. For comparison, the average r for the attenuation is -48.7% and the overall average for r (including both the enhancement and attenuation) is -35.2% (Table 1). Therefore the cloud gap effect represents a substantial compensation for the attenuation of sunlight by clouds. Because of the abnormal distributions, these means are for illustrative purpose only and must be treated cautiously. For example, due to the bimodal pattern, the overall average of the relative change r , which falls between the two peaks, is not a representative indication of effects of clouds on surface irradiance (Fig. 3(A)).

To determine how the patterns, shown in Fig. 3, evolve with time during the day, we divide the daytime into seven periods of equal duration: early morning period, middle morning period, late morning period, noontime period, early afternoon period, middle afternoon period, and late afternoon period. Each period

Table 1
Some statistics on cloud modulation of surface irradiance

	Enhancement only	Attenuation only	Over all
Mean relative change (%)	14.3	-48.7	-35.2
Mean duration (min)	7	24	-

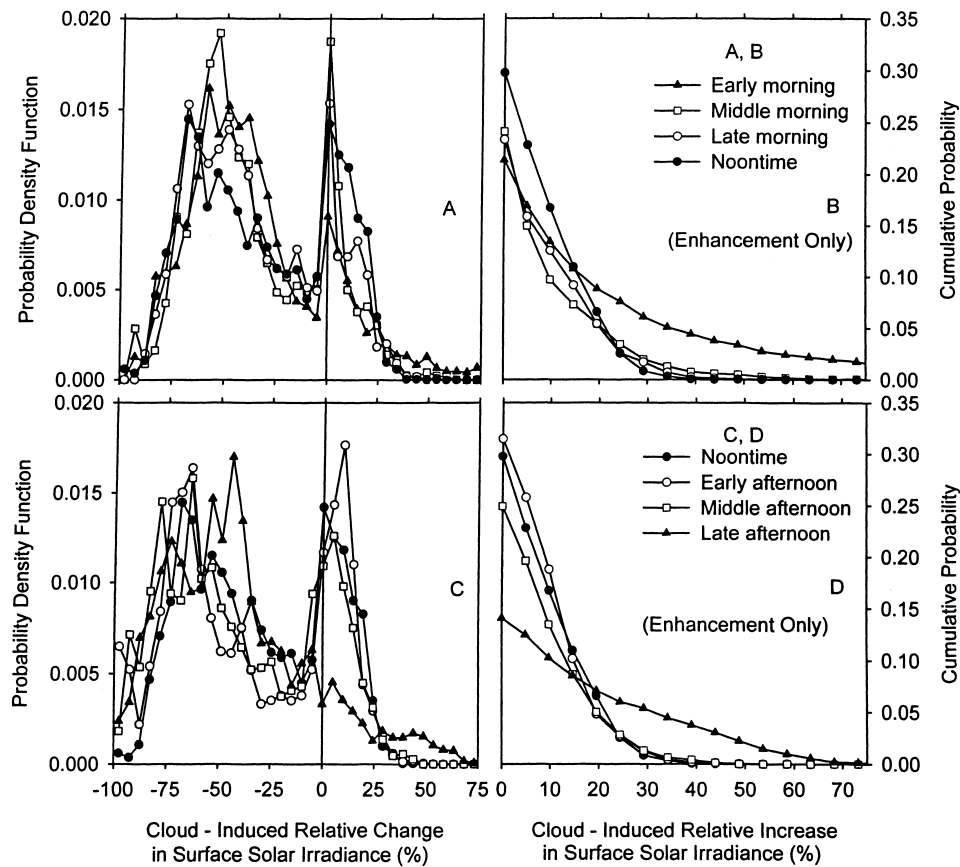


Fig. 4. Probability density functions ((A) and (C)) and cumulative probability distributions ((B) and (D)) of cloud-induced changes in surface solar irradiance relative to the clear-sky level for different periods of the day.

lasts for 1 h and 40 min. For each period, we determine the probability density function and the cumulative probability distribution as in Eq. (9) and (10), respectively. The distributions obtained are shown in Fig. 4. The probability density function exhibits a bimodal characteristic (Fig. 4(A) and (C)) for all periods of the day. However, the shine peak tends to diminish at the low solar elevation angles, especially during the afternoon. The shade peak for the noontime period tends to be smaller than other periods. While the shine peaks for other time periods are centered around the clear-sky irradiance ($r = 0\%$), the shine peaks corresponding to the early and middle afternoon periods are located at the enhancement side ($r > 0\%$).

The cumulative probability distributions for different time periods of the day (Fig. 4(B) and (D)) show that noontime and early afternoon are the time when

the surface irradiance is most likely to be enhanced by clouds ($r > 0\%$). Overall, low solar elevation angles reduce the cumulative probability of surface irradiance enhancement ($r > 0\%$, see the curves for early morning period in Fig. 4(B) and late afternoon period in Fig. 4(D)). For large values of r ($r > 20\%$), however, the early morning and late afternoon periods have higher cumulative probability than other periods of the day. This means that early morning and late afternoon are more likely to experience high relative increases in surface solar irradiance if the cloud gap effect happens. The curves of the cumulative probability distribution for middle morning, late morning, noontime, early afternoon and middle afternoon are fairly close to each other (Fig. 4(B) and (D)). For these periods, the relative change in surface irradiance (r) rarely exceeds 30%.

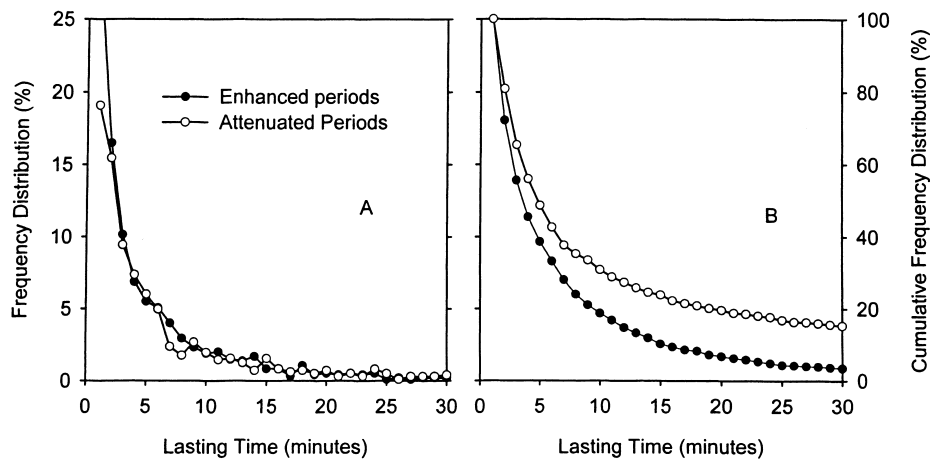


Fig. 5. Frequency distributions (A) and cumulative frequency distributions (B) of the duration of cloud-induced enhancement and attenuation of surface solar irradiance. All degrees of enhancement and attenuation are included.

4.3. Distributions of enhanced and attenuated periods

The periods of enhanced surface solar irradiance were generally short. However, occasionally long periods with enhanced solar irradiance lasting for nearly 1 h were observed. We determined the duration of periods of enhanced and attenuated surface irradiance based on the time when the measured irradiance curve crosses the modeled clear-sky irradiance curve. The distributions (histograms) of these periods were then studied. Fig. 5 shows the frequency distributions (Fig. 5(A)) and cumulative frequency distributions (Fig. 5(B)) of the duration of the enhanced and attenuated periods. For both the enhancement and attenuation, the frequency decreases as the duration increases (Fig. 5(A)). Both distributions exhibit typical hyperbolic features. The initial decrease is fast but the trend becomes very flat after the period exceeds 10 min (Fig. 5(A)). A similar pattern is also shown in the cumulative frequency distributions (Fig. 5(B)). This hyperbolic feature results from the existence of some persistent long periods of surface irradiance enhancement and attenuation in the measurement. It also appears that the attenuation has higher probabilities to experience long duration than the enhancement. This is shown clearly in Fig. 5(B) in which the cumulative frequency distribution curve for the attenuation is above the curve for the enhancement. The

average duration for the enhancement is 7 min while the average duration for the attenuation is 24 min (Table 1). These means, reported here and following, are for illustrative purposes only due to the hyperbolic distributions of involved variables.

To learn, how the duration distributions change with the degrees of enhancement and attenuation, we used the mean relative irradiance change \bar{r} in a given period as an index and separated the distributions into the following categories: $\bar{r} > 20\%$, $10\% < \bar{r} < 20\%$, $0\% < \bar{r} < 10\%$, $-20\% < \bar{r} < 0\%$, $-40\% < \bar{r} < -20\%$, and $\bar{r} < -40\%$. The ranges of these categories were determined based on considerations of including sufficient number of samples in each category. Fig. 6 shows the frequency distributions (histograms, Fig. 6(A) and (C)) and cumulative frequency distributions (Fig. 6(B) and (D)) for these categories. The mean times of duration are given in Table 2. It shows that the mean duration increases as the degree of enhancement or attenuation increases. The peak of the frequency distributions for the attenuation tends to move towards longer duration as the degree of attenuation increases (mean r decreases, Fig. 6(C)).

4.4. Scaling (scale invariant) regimes of surface irradiance

A fast-Fourier transform (FFT) spectral analysis for the time series of surface irradiance was conducted to

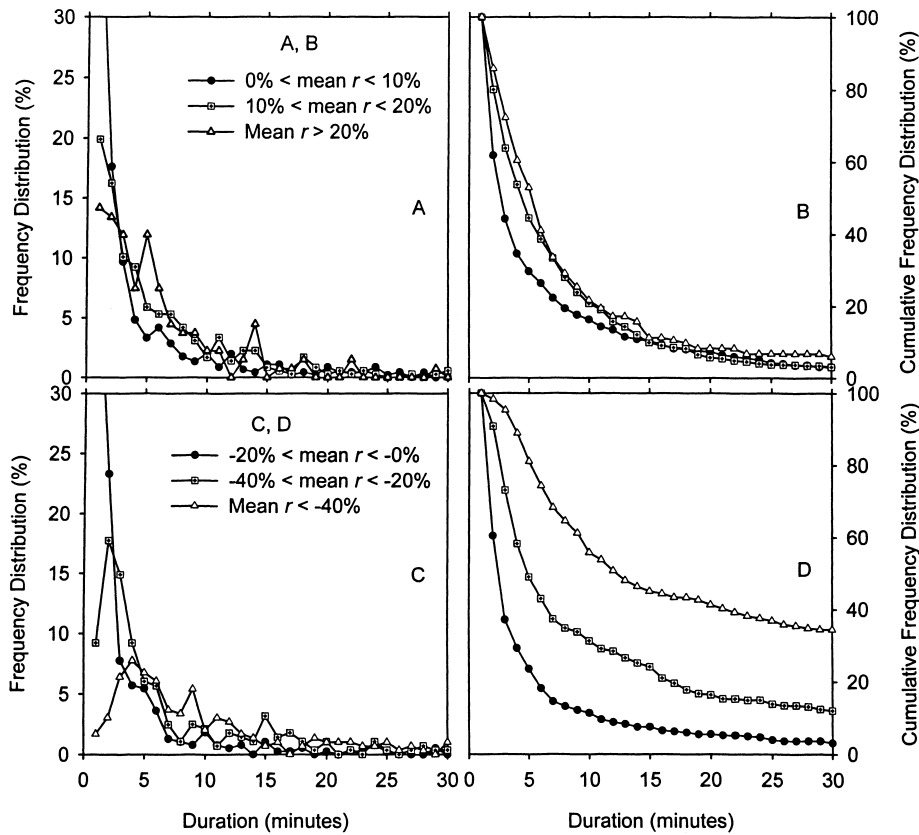


Fig. 6. Frequency distributions ((A) and (C)) and cumulative frequency distributions ((B) and (D)) of the duration of cloud-induced enhancement ((A) and (B)) and attenuation ((C) and (D)) of surface solar irradiance for different degrees of enhancement or attenuation.

determine the characteristic time scales of the modulation of the irradiance by clouds. Measurements of irradiance were continuous from 7 January to 28 February. The FFT was conducted for this period using the Signal Processing Toolbox of MATLAB with a 4-day Bartlett window for spectral averaging. The log–log power spectrum obtained is shown in Fig. 7.

A striking feature of the spectrum is the lack of characteristic time scales other than the two peaks representing harmonics for the diurnal cycle (Fig. 7). In particular, for cycles with periods less than about 9 h,

the log–log spectrum is composed of two nearly linear sections with a smooth transition around 10 min. The linearity indicates a power law relationship between the power spectrum density (PSD) and frequency (f), which in turn reflects invariance of statistical properties under a scale changing operation. For the time scale between 10 min to 9 h, $PSD \sim f^{-1.158}$ with $r^2 = 0.91$. For the time scale smaller than 10 min, the classical Kolmogorov $f^{-5/3}$ law applies with $r^2 = 0.93$. Apparently these two linear sections correspond to two different regimes controlling the cloud-induced

Table 2
Mean duration of periods for different degrees of enhancement and attenuation

Mean relative change (%)	$\bar{r} > 20$	$10 < \bar{r} < 20$	$0 < \bar{r} < 10$	$-20 < \bar{r} < 0$	$-40 < \bar{r} < -20$	$\bar{r} < -40$
Mean duration (min)	9	7	6	6	13	57

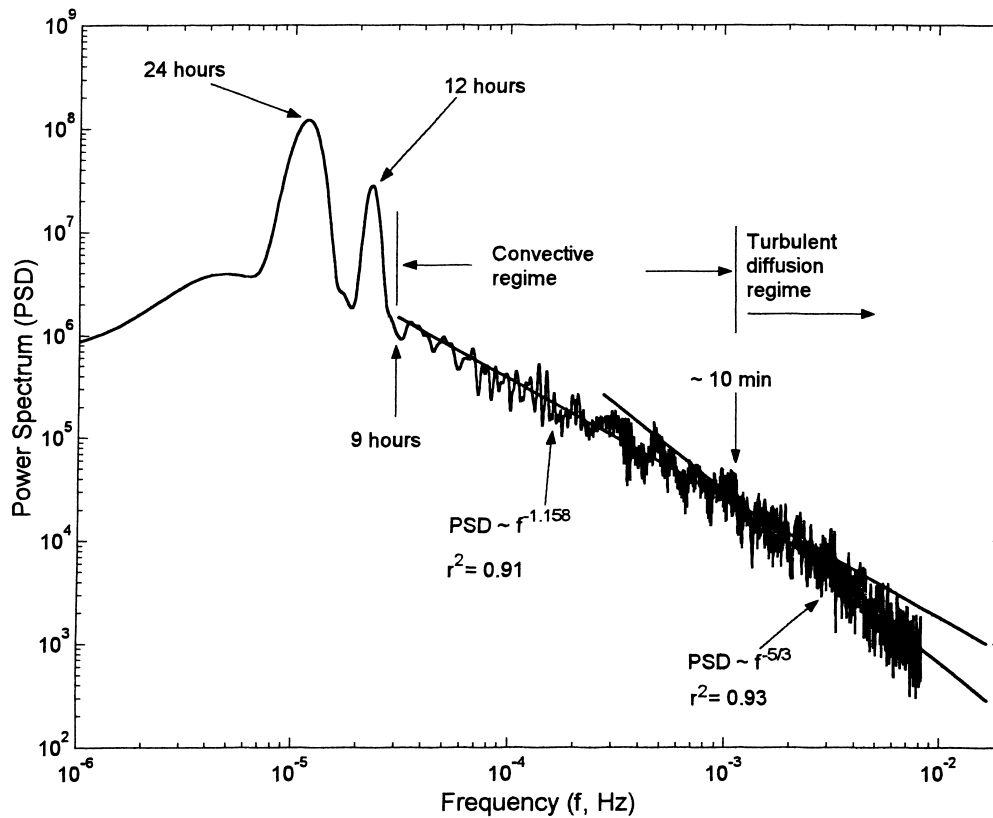


Fig. 7. Power spectrum of the 1 min values of surface solar irradiance from 7 January to 28 February, 1999.

temporal dynamics of surface irradiance. The section from 9 h to 10 min includes convective and mesoscale cloud processes. Small cumulus clouds and the growing and decaying towers within a large cumulus cloud have time scales in the order of 10 min. Ensembles of convective clouds in organized mesoscale systems have durations of tens of minutes to hours. We regard this section of the spectrum as characterizing the convective regime of the cloud systems encountered at the study location. The $-5/3$ slope, characteristic of turbulent processes, with a time scale < 10 min is attributed to the atmospheric turbulence diffusion regime. This regime probably reflects internal inhomogeneities within individual clouds (e.g. variations in liquid water content) and external inhomogeneities in fields composed of relatively small clouds. These internal and external small-scale inhomogeneities create high frequency fluctuations in surface irradiance. These two regimes are discussed in more detail below.

4.5. Influence on surface solar radiative forcing

On a daily basis, the total energy input of the cloud-induced enhancement to surface solar radiative forcing E_g (J m^{-2}) can be determined by Eq. (11)

$$E_g = \int_{\text{sunrise}}^{\text{sunset}} \{\max[I(t), I_c(t)] - I_c(t)\} dt \quad (11)$$

The total solar energy attenuated by clouds during a day E_a is determined from Eq. (12)

$$E_a = \int_{\text{sunrise}}^{\text{sunset}} \{I_c(t) - \min[I(t), I_c(t)]\} dt \quad (12)$$

Finally, the total daily surface solar radiative forcing E_t is given by Eq. (13)

$$E_t = \int_{\text{sunrise}}^{\text{sunset}} I(t) dt \quad (13)$$

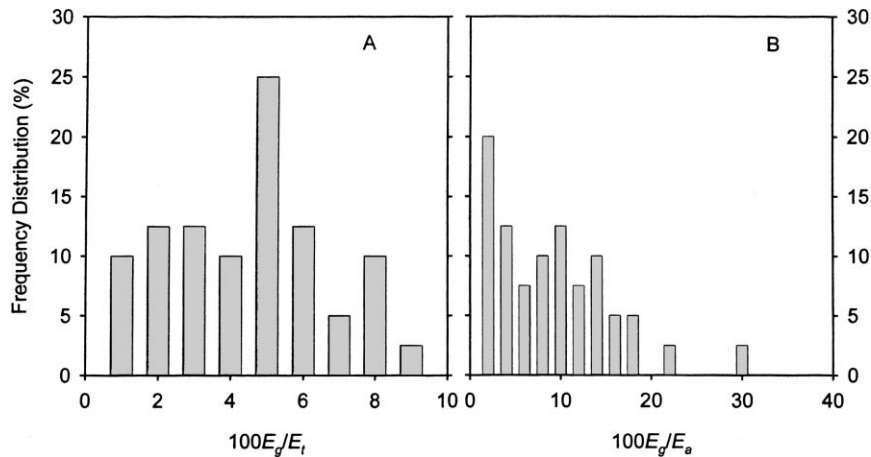


Fig. 8. Frequency distributions of the percentages of daily total solar energy contribution from cloud gap effect relative to daily total solar energy received by the ground surface (A) and the percentages of this energy contribution relative to daily total solar energy attenuated by clouds (B).

The magnitudes of E_g relative to E_a and E_t ($100E_g/E_t$ and $100E_g/E_a$, respectively) are determined from our measurements. Fig. 8 shows the histograms of these two percentages. The frequency distribution of $100E_g/E_t$ has a peak around 5% (Fig. 8(A)). Averaged over the 2-month period of our measurements, the cloud-induced surface irradiance enhancement contributed $4.0 \pm 0.4\%$ of daily solar energy input onto the ground surface. The frequency distribution of $100E_g/E_a$ apparently has multiple peaks (Fig. 8(B)). On a daily basis, the energy input to the ground surface due to the cloud-induced surface irradiance enhancement averaged over the 2-month period amounted to $11.7 \pm 2.7\%$ of the solar energy attenuated by the clouds.

5. Summary and conclusions

Clouds modulate surface solar radiation in a complex manner with two seemingly contradictory aspects. The commonsense aspect is that overhead clouds reduce surface irradiance. The peak distribution of relative change r around -60% indicates that dominant clouds during our measurement periods were optically thick (Fig. 3(A) and Fig. 4(A) and (C)). Less obvious is that clouds, especially cumuloform clouds, can enhance surface irradiance to such a

degree that the extraterrestrial irradiance is exceeded. The enhancement was a pervasive phenomenon in our observations. It covered almost a quarter of our daily irradiance measurements or equivalently a quarter of daily time (one datum represents 1 min, Fig. 3(B) and Fig. 4(B) and (D)). The energy contribution from the cloud gap effect to the solar radiative forcing at the surface was not trivial. It accounted for 4.0% of the daily solar radiative forcing at the surface and compensated for 11.7% of solar energy attenuation by clouds.

The duration of most periods of surface irradiance enhancement was on the order of several minutes. This is sufficiently long to impact many atmospheric chemical processes. For example, molecular cleavage by photolysis can occur at temporal scales less than one minute (Brasseur et al., 1999, pp. 112–113). However, it is probably not long enough for stomata of plants to have a full response since stomatal conductance may take 30–60 min to reach equilibrium (Mansfield and Heath, 1963; Mansfield and Meidner, 1966). Nevertheless this does not preclude the potential importance of the cloud gap effect in affecting biophysical processes of vegetative ecosystems since for a rapidly changing radiation environment in which cloud gap effect is associated (Fig. 2), equilibrium in stomatal openness cannot be achieved regardless of whether it is in the period of irradiance enhancement

or attenuation. Another important factor is the diffusive nature of the part of the surface solar irradiance in excess of the clear-sky level. Plant canopies have higher photosynthetic use efficiencies for diffuse radiation than for direct beam radiation (Wang and Jarvis, 1990; Gu et al., 1999). The biophysical importance of cloud gap effect was already revealed in Gu et al. (1999). They found that cloud gap effect led to higher photosynthetic rate of two boreal deciduous forests.

Although data are unavailable to us for analyzing spatial heterogeneity in surface solar irradiance, the findings presented here cast some insights into the mosaic radiative landscape created by cloud fields. The magnitude of the fluctuation in the time series is a reflection of the magnitude of spatial variability. As shown in our time series, the differences between local minima and maxima of successive shaded and sunlit periods often exceeded the magnitude of the corresponding clear-sky surface irradiance. If the irradiance differences between sunlit and sun-shaded areas have this magnitude, large horizontal heterogeneities in exchanges of carbon dioxide, sensible heat and water vapor can be created even for horizontally homogeneous ecosystems. If the heterogeneities induced by cloud fields fall within the footprints of flux towers, the interpretation of flux measurements can be complicated.

It appears that this study is the first to report that modulations of surface solar irradiance by clouds can be characterized by a convective regime and a turbulence diffusion regime (Fig. 7). The convective regime is responsible for fluctuations of relatively long time periods while the turbulence diffusion regime controls fluctuations of relatively short time periods. Fields of fair-weather cumulus, common from about 10 am to midday (local time), are comprised of clouds which are approximately cubic in dimensions with sides in the order of 1–2 km. Dominant radiative signals at 3 min suggest that such clouds are embedded in a velocity field of 5–10 m s⁻¹. Cloud-free air spaces would then correspond to linear dimensions similar to the size of the clouds. Once development sets in and deeper convective clouds form, the vertical dimensions of the cumulus congestus and cumulonimbus are likely to exceed their horizontal dimensions reaching heights of 15–18 km. Cloud ensembles and mesoscale convective systems become organized and persist for numbers of hours.

It is well known that when a passive scalar is introduced into a turbulent fluid, the spectrum of its fluctuations is generically described by the Kolmogorov $f^{-5/3}$ law. The observed $-5/3$ power law in the spectrum of surface irradiance suggests that scattering from the vertical sides of the cumulus clouds is a function of the turbulent motions involved in the three dimensional mixing which takes place on these cloud walls.

Acknowledgements

We are grateful for the field infrastructure and financial support that NASA provided to achieve this study through TRMM-LBA project. We also thank our Brazilian colleagues Dr. Gilberto Fisch and Jorge Oliveira (Centro Técnico Aeroespacial, São José dos Campos) for their assistance with the field measurements. Data analysis was supported by the NASA grants NAG5-6421 (Global Vegetation Dynamics) and NAG5-7956 (Land-Surface Characterization of South African Savannas). We greatly benefited from discussions with and comments of our colleague B. Hayden. Finally, we thank two journal anonymous reviewers for their comments to improve the manuscript.

References

- Brasseur, G.P., Orlando, J.J., Tyndall, G.S., 1999. Atmospheric Chemistry and Global Change. Oxford University Press, New York, USA, p. 654.
- Duchon, C.E., O'Malley, M.S., 1999. Estimating cloud type from pyranometer observations. *J. Appl. Meteor.* 38, 132–141.
- Garstang, M., Fitzjarrald, D., 1999. Observations of Surface to Atmosphere Interactions in the Tropics. Oxford University Press, New York, USA, p. 405.
- Gu, L., Fuentes, J.D., Shugart, H.H., Staebler, R.M., Black, T.A., 1999. Responses of net ecosystem exchanges of carbon dioxide to changes in cloudiness: results from two North American deciduous forests. *J. Geophys. Res.* 104, 31421–31434.
- Ibqal, M., 1983. An Introduction to Solar Radiation. Academic Press, p. 390.
- Mansfield, T.A., Heath, O.V.S., 1963. Studies in stomatal behaviour. X. An investigation of responses to low intensity illumination and temperature in *Xanthium pennsylvanicum*. *J. Exp. Bot.* 15, 114–124.
- Mansfield, T.A., Meidner, H., 1966. Stomatal opening in light of different wavelengths: effects of blue light independent of carbon dioxide concentration. *J. Exp. Bot.* 17, 510–521.

- Meyers, T.P., Dale, R.F., 1983. Predicting daily insolation with hourly cloud heights and coverage. *J. Climate Appl. Meteor.* 22, 537–545.
- Michalsky, J.J., 1988. The Astronomical Almanac's algorithm for approximate solar position (1950–2050). *Solar Energy* 40, 227–235.
- Press, W.H., Teukolsky, S.A., Vetterling, W.T., Flannery, B.P., 1992. *Numerical Recipes in FORTRAN — The Art of Scientific Computing*, 2nd Edition. Cambridge University Press, New York, p. 963.
- Segal, M., Davis, J., 1992. The impact of deep cumulus reflection on the ground-level global irradiance. *J. Appl. Meteor.* 31, 217–222.
- Smith, W.L., 1966. Note on the relationship between total precipitable water and surface dewpoint. *J. Appl. Meteor.* 5, 726–727.
- Wang, Y.P., Jarvis, P., 1990. Effect of incident beam and diffuse radiation on PAR absorption, photosynthesis, and transpiration of sitka spruce — a simulation study. *Silva Carelica* 15, 167–180.